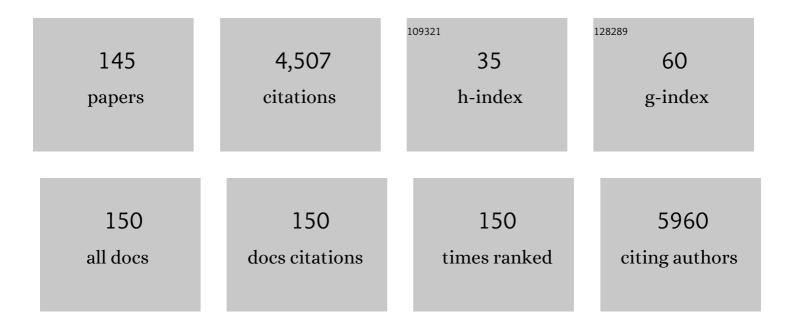
Byeong-Cheol Ahn

List of Publications by Year in descending order

Source: https://exaly.com/author-pdf/1293020/publications.pdf Version: 2024-02-01



BYFONC-CHEOLAHN

#	Article	IF	CITATIONS
1	Tunable fluorescent carbon dots from biowaste as fluorescence ink and imaging human normal and cancer cells. Environmental Research, 2022, 204, 112365.	7.5	78
2	An Update on the Effectiveness of Probiotics in the Prevention and Treatment of Cancer. Life, 2022, 12, 59.	2.4	24
3	KSNM60 in Nuclear Endocrinology: from the Beginning to the Future. Nuclear Medicine and Molecular Imaging, 2022, 56, 17-28.	1.0	2
4	Reliability of Alkaline Phosphatase for Differentiating Flare Phenomenon from Disease Progression with Bone Scintigraphy. Cancers, 2022, 14, 254.	3.7	5
5	Hepatoprotective Potential of Malaysian Medicinal Plants: A Review on Phytochemicals, Oxidative Stress, and Antioxidant Mechanisms. Molecules, 2022, 27, 1533.	3.8	20
6	Advancing Regenerative Cellular Therapies in Non-Scarring Alopecia. Pharmaceutics, 2022, 14, 612.	4.5	12
7	Targeting GLI1 Transcription Factor for Restoring lodine Avidity with Redifferentiation in Radioactive-lodine Refractory Thyroid Cancers. Cancers, 2022, 14, 1782.	3.7	1
8	Evolution of Mesenchymal Stem Cell Therapy as an Advanced Therapeutic Medicinal Product (ATMP)—An Indian Perspective. Bioengineering, 2022, 9, 111.	3.5	9
9	Lineage Differentiation Potential of Different Sources of Mesenchymal Stem Cells for Osteoarthritis Knee. Pharmaceuticals, 2022, 15, 386.	3.8	5
10	Convalescent serum-derived exosomes: Attractive niche as COVID-19 diagnostic tool and vehicle for mRNA delivery. Experimental Biology and Medicine, 2022, 247, 1244-1252.	2.4	15
11	Application of Sygen® in Diabetic Peripheral Neuropathies—A Review of Biological Interactions. Bioengineering, 2022, 9, 217.	3.5	2
12	Identification of Angiogenic Cargoes in Human Fibroblasts-Derived Extracellular Vesicles and Induction of Wound Healing. Pharmaceuticals, 2022, 15, 702.	3.8	5
13	Current understanding of MSC-derived exosomes in the management of knee osteoarthritis. Experimental Cell Research, 2022, 418, 113274.	2.6	13
14	Extracellular vesicles derived from fibroblasts promote wound healing by optimizing fibroblast and endothelial cellular functions. Stem Cells, 2021, 39, 266-279.	3.2	29
15	Sentinel lymph node biopsy in acral melanoma: A Korean single enter experience with 107 patients (2006–2018). Asia-Pacific Journal of Clinical Oncology, 2021, 17, 115-122.	1.1	4
16	Self-healing functionalization of sulfonated hafnium oxide and copper oxide nanocomposite for effective biocidal control of multidrug-resistant bacteria. New Journal of Chemistry, 2021, 45, 9506-9517.	2.8	12
17	Molecular mechanisms of radioactive iodine refractoriness in differentiated thyroid cancer: Impaired sodium iodide symporter (NIS) expression owing to altered signaling pathway activity and intracellular localization of NIS. Theranostics, 2021, 11, 6251-6277.	10.0	59
18	Human fibroblastâ€derived extracellular vesicles promote hair growth in cultured human hair follicles. FEBS Letters, 2021, 595, 942-953.	2.8	12

#	Article	IF	CITATIONS
19	Extracellular Vesicles Act as Nano-Transporters of Tyrosine Kinase Inhibitors to Revert Iodine Avidity in Thyroid Cancer. Pharmaceutics, 2021, 13, 248.	4.5	14
20	Radioiodine labeling and in vivo trafficking of extracellular vesicles. Scientific Reports, 2021, 11, 5041.	3.3	7
21	Identification of Angiogenic Cargo in Extracellular Vesicles Secreted from Human Adipose Tissue-Derived Stem Cells and Induction of Angiogenesis In Vitro and In Vivo. Pharmaceutics, 2021, 13, 495.	4.5	18
22	Noncovalent Functionalized Graphene Nanocarriers from Graphite for Treating Thyroid Cancer Cells. ACS Biomaterials Science and Engineering, 2021, 7, 2317-2328.	5.2	7
23	Clinical Outcome of Parotid Cland Massage for Preventing Parotid Gland Dysfunction in Patients Treated with Radioiodine Therapy for Differentiated Thyroid Cancer: a Prospective Longitudinal Follow-Up Study. International Journal of Thyroidology, 2021, 14, 6-17.	0.1	1
24	NTRK and RET fusion–directed therapy in pediatric thyroid cancer yields a tumor response and radioiodine uptake. Journal of Clinical Investigation, 2021, 131, .	8.2	62
25	Engineered extracellular vesicle mimetics from macrophage promotes hair growth in mice and promotes human hair follicle growth. Experimental Cell Research, 2021, 409, 112887.	2.6	8
26	Osteogenic and Chondrogenic Potential of Periosteum-Derived Mesenchymal Stromal Cells: Do They Hold the Key to the Future?. Pharmaceuticals, 2021, 14, 1133.	3.8	8
27	Reappraisal of bone scintigraphy as a new tool for the evaluation of disease activity in patients with rheumatoid arthritis. Scientific Reports, 2021, 11, 21809.	3.3	1
28	Treatment Effect of Combining Lenvatinib and Vemurafenib for BRAF Mutated Anaplastic Thyroid Cancer. International Journal of Thyroidology, 2021, 14, 127-134.	0.1	0
29	Is Culture Expansion Necessary in Autologous Mesenchymal Stromal Cell Therapy to Obtain Superior Results in the Management of Knee Osteoarthritis?—Meta-Analysis of Randomized Controlled Trials. Bioengineering, 2021, 8, 220.	3.5	6
30	White blood cell labeling with Technetium-99m (99mTc) using red blood cell extracellular vesicles-mimetics. Blood Cells, Molecules, and Diseases, 2020, 80, 102375.	1.4	15
31	Lenvatinib for Radioactive Iodine-Refractory Differentiated Thyroid Carcinoma and Candidate Biomarkers Associated with Survival: A Multicenter Study in Korea. Thyroid, 2020, 30, 732-738.	4.5	28
32	An Efficient Region Precise Thresholding and Direct Hough Transform in Femur and Femoral Neck Segmentation Using Pelvis CT. IEEE Access, 2020, 8, 110048-110058.	4.2	7
33	Role of M2-like macrophages in the progression of ovarian cancer. Experimental Cell Research, 2020, 395, 112211.	2.6	13
34	Deep learning enables automated localization of the metastatic lymph node for thyroid cancer on 1311 post-ablation whole-body planar scans. Scientific Reports, 2020, 10, 7738.	3.3	8
35	Extracellular Vesicle- and Extracellular Vesicle Mimetics-Based Drug Delivery Systems: New Perspectives, Challenges, and Clinical Developments. Pharmaceutics, 2020, 12, 442.	4.5	77
36	Application of In Vivo Imaging Techniques for Monitoring Natural Killer Cell Migration and Tumor Infiltration. Cancers, 2020, 12, 1318.	3.7	8

#	Article	IF	CITATIONS
37	Extracellular vesicles derived from macrophage promote angiogenesis In vitro and accelerate new vasculature formation In vivo. Experimental Cell Research, 2020, 394, 112146.	2.6	28
38	A new tyrosine kinase inhibitor K905-0266 inhibits proliferation and sphere formation of glioblastoma cancer cells. Journal of Drug Targeting, 2020, 28, 933-938.	4.4	1
39	Reduction of Salivary Gland Damage During Radioiodine Therapy for Differentiated Thyroid Cancers. Nuclear Medicine and Molecular Imaging, 2020, 54, 126-127.	1.0	2
40	A Novel Tyrosine Kinase Inhibitor Can Augment Radioactive Iodine Uptake Through Endogenous Sodium/Iodide Symporter Expression in Anaplastic Thyroid Cancer. Thyroid, 2020, 30, 501-518.	4.5	18
41	Macrophage-Derived Extracellular Vesicle Promotes Hair Growth. Cells, 2020, 9, 856.	4.1	60
42	In Vivo Tracking of Tumor-Derived Bioluminescent Extracellular Vesicles in Mice. Methods in Molecular Biology, 2020, 2081, 203-210.	0.9	4
43	Noninvasive <i>in vivo</i> cell tracking using molecular imaging: A useful tool for developing mesenchymal stem cell-based cancer treatment. World Journal of Stem Cells, 2020, 12, 1492-1510.	2.8	9
44	F-18 FDG PET for assessment of disease activity of large vessel vasculitis: A systematic review and meta-analysis. Journal of Nuclear Cardiology, 2019, 26, 59-67.	2.1	31
45	Lesion-Based Evaluation Predicts Treatment Response to Lenvatinib for Radioactive Iodine-Refractory Differentiated Thyroid Cancer: A Korean Multicenter Retrospective Study. Thyroid, 2019, 29, 1811-1819.	4.5	19
46	Enhancing prognosis prediction using pre-treatment nodal SUVmax and HPV status in cervical squamous cell carcinoma. Cancer Imaging, 2019, 19, 43.	2.8	8
47	Role of thyroglobulin in the management of patients with differentiated thyroid cancer. Clinical and Translational Imaging, 2019, 7, 209-217.	2.1	2
48	Clinical outcomes of patients with T4 or N1b well-differentiated thyroid cancer after different strategies of adjuvant radioiodine therapy. Scientific Reports, 2019, 9, 5570.	3.3	12
49	<p>A novel strategy of transferring NIS protein to cells using extracellular vesicles leads to increase in iodine uptake and cytotoxicity</p> . International Journal of Nanomedicine, 2019, Volume 14, 1779-1787.	6.7	22
50	Combination Treatment with the <i>BRAF^{V600E}</i> Inhibitor Vemurafenib and the BH3 Mimetic Navitoclax for <i>BRAF</i> -Mutant Thyroid Carcinoma. Thyroid, 2019, 29, 540-548.	4.5	13
51	Exosomes derived from human dermal papilla cells promote hair growth in cultured human hair follicles and augment the hairâ€inductive capacity of cultured dermal papilla spheres. Experimental Dermatology, 2019, 28, 854-857.	2.9	83
52	Development and Validation of an ¹⁸ Fâ€Fluorodeoxyglucose–Positron Emission Tomography With Computed Tomography–Based Tool for the Evaluation of Joint Counts and Disease Activity in Patients With Rheumatoid Arthritis. Arthritis and Rheumatology, 2019, 71, 1232-1240.	5.6	26
53	The Preventive Effect of Parotid Gland Massage on Salivary Gland Dysfunction During High-Dose Radioactive Iodine Therapy for Differentiated Thyroid Cancer. Clinical Nuclear Medicine, 2019, 44, 625-633.	1.3	18
54	Serum thyroglobulin elevation after needle aspiration of the lymph nodes: the predictive value for detecting metastasis in papillary thyroid cancer patients – a pilot study. Medicine (United States), 2019, 98, e16461.	1.0	4

#	Article	IF	CITATIONS
55	Enhancement of antitumor potency of extracellular vesicles derived from natural killer cells by IL-15 priming. Biomaterials, 2019, 190-191, 38-50.	11.4	87
56	In vivo migration of mesenchymal stem cells to burn injury sites and their therapeutic effects in a living mouse model. Journal of Controlled Release, 2018, 279, 79-88.	9.9	72
57	Factors Associated with Dose Determination of Radioactive Iodine Therapy for Differentiated Thyroid Cancer. Nuclear Medicine and Molecular Imaging, 2018, 52, 247-253.	1.0	10
58	Optimization of Dendritic Cell-Mediated Cytotoxic T-Cell Activation by Tracking of Dendritic Cell Migration Using Reporter Gene Imaging. Molecular Imaging and Biology, 2018, 20, 398-406.	2.6	6
59	Management of Severe Fatigue Induced by Tyrosine Kinase Inhibitor in Radioiodine Refractory Thyroid Cancer. International Journal of Thyroidology, 2018, 11, 75.	0.1	Ο
60	Prognostic value of 18F-fluorodeoxyglucose bone marrow uptake in patients with solid tumors. Medicine (United States), 2018, 97, e12859.	1.0	8
61	Reverting iodine avidity of radioactive-iodine refractory thyroid cancer with a new tyrosine kinase inhibitor (K905-0266) excavated by high-throughput NIS (sodium iodide symporter) enhancer screening platform using dual reporter gene system. Oncotarget, 2018, 9, 7075-7087.	1.8	20
62	New Optical Imaging Reporter-labeled Anaplastic Thyroid Cancer-Derived Extracellular Vesicles as a Platform for In Vivo Tumor Targeting in a Mouse Model. Scientific Reports, 2018, 8, 13509.	3.3	17
63	A New Approach for Loading Anticancer Drugs Into Mesenchymal Stem Cell-Derived Exosome Mimetics for Cancer Therapy. Frontiers in Pharmacology, 2018, 9, 1116.	3.5	179
64	An Update on in Vivo Imaging of Extracellular Vesicles as Drug Delivery Vehicles. Frontiers in Pharmacology, 2018, 9, 169.	3.5	110
65	Migration of mesenchymal stem cells to tumor xenograft models and <i>in vitro</i> drug delivery by doxorubicin. International Journal of Medical Sciences, 2018, 15, 1051-1061.	2.5	45
66	Regulated Mesenchymal Stem Cells Mediated Colon Cancer Therapy Assessed by Reporter Gene Based Optical Imaging. International Journal of Molecular Sciences, 2018, 19, 1002.	4.1	16
67	Prevalence and Risk Factors of Atypical Femoral Fracture Bone Scintigraphic Feature in Patients Experiencing Bisphosphonate-Related Osteonecrosis of the Jaw. Nuclear Medicine and Molecular Imaging, 2018, 52, 311-317.	1.0	2
68	Targeting and Therapy of Glioblastoma in a Mouse Model Using Exosomes Derived From Natural Killer Cells. Frontiers in Immunology, 2018, 9, 824.	4.8	77
69	Risk factors for radioactive iodine-avid metastatic lymph nodes on post I-131 ablation SPECT/CT in low- or intermediate-risk groups of papillary thyroid cancer. PLoS ONE, 2018, 13, e0202644.	2.5	8
70	In vivo Non-invasive Imaging of Radio-Labeled Exosome-Mimetics Derived From Red Blood Cells in Mice. Frontiers in Pharmacology, 2018, 9, 817.	3.5	72
71	Contribution of Radionuclide Theranostics for Managing Intractable Malignancies. Nuclear Medicine and Molecular Imaging, 2018, 52, 168-169.	1.0	2
72	Novel alternatives to extracellular vesicle-based immunotherapy – exosome mimetics derived from natural killer cells. Artificial Cells, Nanomedicine and Biotechnology, 2018, 46, 166-179.	2.8	74

#	Article	IF	CITATIONS
73	Early perfusion and dopamine transporter imaging using F-FP-CIT PET/CT in patients with parkinsonism. American Journal of Nuclear Medicine and Molecular Imaging, 2018, 8, 360-372.	1.0	15
74	Multimodality Imaging of Bone Marrow–Derived Dendritic Cell Migration and Antitumor Immunity. Translational Oncology, 2017, 10, 262-270.	3.7	14
75	Clinical outcomes of low-dose and high-dose postoperative radioiodine therapy in patients with intermediate-risk differentiated thyroid cancer. Nuclear Medicine Communications, 2017, 38, 228-233.	1.1	27
76	High Prevalence of Thyroid Disease and Role of Salivary Gland Scintigraphy in Patients with Xerostomia. Nuclear Medicine and Molecular Imaging, 2017, 51, 169-177.	1.0	10
77	Development of an athyroid mouse model using 1311 ablation after preparation with a low-iodine diet. Scientific Reports, 2017, 7, 13284.	3.3	7
78	Extracellular vesicles from mesenchymal stem cells activates VEGF receptors and accelerates recovery of hindlimb ischemia. Journal of Controlled Release, 2017, 264, 112-126.	9.9	164
79	Re. Clinical Nuclear Medicine, 2017, 42, 241.	1.3	0
80	Extracellular vesicles derived from MSCs activates dermal papilla cell in vitro and promotes hair follicle conversion from telogen to anagen in mice. Scientific Reports, 2017, 7, 15560.	3.3	123
81	I-131 biokinetics of remnant normal thyroid tissue and residual thyroid cancer in patients with differentiated thyroid cancer: comparison between recombinant human TSH administration and thyroid hormone withdrawal. Annals of Nuclear Medicine, 2017, 31, 582-589.	2.2	15
82	Nuclear Medicine in the Era of Precision Medicine. Nuclear Medicine and Molecular Imaging, 2017, 51, 99-100.	1.0	12
83	Non-invasive visualization of mast cell recruitment and its effects in lung cancer by optical reporter gene imaging and glucose metabolism monitoring. Biomaterials, 2017, 112, 192-203.	11.4	5
84	Visualization of Macrophage Recruitment to Inflammation Lesions using Highly Sensitive and Stable Radionuclide-Embedded Gold Nanoparticles as a Nuclear Bio-Imaging Platform. Theranostics, 2017, 7, 926-934.	10.0	29
85	Exosomes Derived From Natural Killer Cells Exert Therapeutic Effect in Melanoma. Theranostics, 2017, 7, 2732-2745.	10.0	328
86	Redifferentiation of Radioiodine Refractory Differentiated Thyroid Cancer for Reapplication of I-131 Therapy. Frontiers in Endocrinology, 2017, 8, 260.	3.5	48
87	Natural Killer Cell (NK-92MI)-Based Therapy for Pulmonary Metastasis of Anaplastic Thyroid Cancer in a Nude Mouse Model. Frontiers in Immunology, 2017, 8, 816.	4.8	44
88	Molecular Imaging: A Useful Tool for the Development of Natural Killer Cell-Based Immunotherapies. Frontiers in Immunology, 2017, 8, 1090.	4.8	40
89	In Vivo Tracking of Chemokine Receptor CXCR4-Engineered Mesenchymal Stem Cell Migration by Optical Molecular Imaging. Stem Cells International, 2017, 2017, 1-10.	2.5	60
90	Current Perspectives on In Vivo Noninvasive Tracking of Extracellular Vesicles with Molecular Imaging. BioMed Research International, 2017, 2017, 1-11.	1.9	94

#	Article	IF	CITATIONS
91	Genetically engineered suicide gene in mesenchymal stem cells using a Tet-On system for anaplastic thyroid cancer. PLoS ONE, 2017, 12, e0181318.	2.5	15
92	Deep vector-based convolutional neural network approach for automatic recognition of colonies of induced pluripotent stem cells. PLoS ONE, 2017, 12, e0189974.	2.5	43
93	Drug Discovery by Molecular Imaging and Monitoring Therapy Response in Lymphoma. International Journal of Molecular Sciences, 2017, 18, 1639.	4.1	22
94	A new bioluminescent reporter system to study the biodistribution of systematically injected tumor-derived bioluminescent extracellular vesicles in mice. Oncotarget, 2017, 8, 109894-109914.	1.8	96
95	Pathological N1b Node Metastasis Itself Can Be Still a Valid Prognostic Factor in PTC after High Dose RAI Therapy. International Journal of Thyroidology, 2016, 9, 159.	0.1	2
96	Advances in Molecular Imaging Strategies for <i>In Vivo</i> Tracking of Immune Cells. BioMed Research International, 2016, 2016, 1-10.	1.9	56
97	Personalized Medicine Based on Theranostic Radioiodine Molecular Imaging for Differentiated Thyroid Cancer. BioMed Research International, 2016, 2016, 1-9.	1.9	49
98	Retrosternal Goiter Visualized on 99mTc Pertechnetate SPECT/CT, But Not on Planar Scintigraphy. Clinical Nuclear Medicine, 2016, 41, e169-e170.	1.3	8
99	Visualization of the Biological Behavior of Tumor-Associated Macrophages in Living Mice with Colon Cancer Using Multimodal Optical Reporter Gene Imaging. Neoplasia, 2016, 18, 133-141.	5.3	21
100	Development of Drugs and Technology for Radiation Theragnosis. Nuclear Engineering and Technology, 2016, 48, 597-607.	2.3	7
101	<scp>R</scp> ole of pulmonary macrophages in initiation of lung metastasis in anaplastic thyroid cancer. International Journal of Cancer, 2016, 139, 2583-2592.	5.1	23
102	Combined Positron Emission Tomography and Cerenkov Luminescence Imaging of Sentinel Lymph Nodes Using PEGylated Radionuclideâ€Embedded Gold Nanoparticles. Small, 2016, 12, 4894-4901.	10.0	34
103	In Vivo therapeutic potential of mesenchymal stem cell-derived extracellular vesicles with optical imaging reporter in tumor mice model. Scientific Reports, 2016, 6, 30418.	3.3	61
104	Multimodality Molecular Imaging of Cardiac Cell Transplantation: Part I. Reporter Gene Design, Characterization, and Optical in Vivo Imaging of Bone Marrow Stromal Cells after Myocardial Infarction. Radiology, 2016, 280, 815-825.	7.3	12
105	Multimodality Molecular Imaging of Cardiac Cell Transplantation: Part II. In Vivo Imaging of Bone Marrow Stromal Cells in Swine with PET/CT and MR Imaging. Radiology, 2016, 280, 826-836.	7.3	12
106	Radionuclide-embedded gold nanoparticles for enhanced dendritic cell-based cancer immunotherapy, sensitive and quantitative tracking of dendritic cells with PET and Cerenkov luminescence. NPG Asia Materials, 2016, 8, e281-e281.	7.9	51
107	Turn-off fluorescence sensor for the detection of ferric ion in water using green synthesized N-doped carbon dots and its bio-imaging. Journal of Photochemistry and Photobiology B: Biology, 2016, 158, 235-242.	3.8	271
108	Tracking of dendritic cell migration into lymph nodes using molecular imaging with sodium iodide symporter and enhanced firefly luciferase genes. Scientific Reports, 2015, 5, 9865.	3.3	43

#	Article	IF	CITATIONS
109	Analysis of Clinical Factors for the Determination of Optimal Serum Level of Thyrotropin After Recombinant Human Thyroid-Stimulating Hormone Administration. Nuclear Medicine and Molecular Imaging, 2015, 49, 268-275.	1.0	9
110	Biological Production of an Integrinαvβ3 Targeting Imaging Probe and Functional Verification. BioMed Research International, 2015, 2015, 1-8.	1.9	6
111	Potential Therapeutic Effect of Natural Killer Cells on Doxorubicin-Resistant Breast Cancer Cells In Vitro. PLoS ONE, 2015, 10, e0136209.	2.5	11
112	Inverse Agonist of Estrogen-Related Receptor γ Enhances Sodium Iodide Symporter Function Through Mitogen-Activated Protein Kinase Signaling in Anaplastic Thyroid Cancer Cells. Journal of Nuclear Medicine, 2015, 56, 1690-1696.	5.0	38
113	Size measurement of the thyroid gland on a magnified pinhole thyroid scan using an ultrasonic device measuring distance from the pinhole to the thyroid gland. Annals of Nuclear Medicine, 2015, 29, 111-117.	2.2	Ο
114	Combined Fluorescence and Magnetic Resonance Imaging of Primary Macrophage Migration to Sites of Acute Inflammation Using Near-Infrared Fluorescent Magnetic Nanoparticles. Molecular Imaging and Biology, 2015, 17, 643-651.	2.6	14
115	Radioiodine Scan Index: A Simplified, Quantitative Treatment Response Parameter for Metastatic Thyroid Carcinoma. Nuclear Medicine and Molecular Imaging, 2015, 49, 174-181.	1.0	8
116	In Vivo Cell Tracking with Bioluminescence Imaging. Nuclear Medicine and Molecular Imaging, 2015, 49, 3-10.	1.0	130
117	Preoperative Prediction of Cervical Lymph Node Metastasis Using Primary Tumor SUVmax on 18F-FDG PET/CT in Patients with Papillary Thyroid Carcinoma. PLoS ONE, 2015, 10, e0144152.	2.5	19
118	Clinical applications of <scp>SPECT</scp> / <scp>CT</scp> after first lâ€131 ablation in patients with differentiated thyroid cancer. Clinical Endocrinology, 2014, 81, 445-451.	2.4	31
119	Emptying effect of massage on parotid gland radioiodine content. Nuclear Medicine Communications, 2014, 35, 1127-1131.	1.1	11
120	Superiority of delayed risk stratification in differentiated thyroid cancer after total thyroidectomy and radioactive iodine ablation. Nuclear Medicine Communications, 2014, 35, 1119-1126.	1.1	27
121	Difference of Clinical and Radiological Characteristics According to Radioiodine Avidity in Pulmonary Metastases of Differentiated Thyroid Cancer. Nuclear Medicine and Molecular Imaging, 2014, 48, 55-62.	1.0	16
122	Requisites for successful theranostics with radionuclide-based reporter gene imaging. Journal of Drug Targeting, 2014, 22, 295-303.	4.4	28
123	Noninvasive Reporter Gene Imaging of Human Oct4 (Pluripotency) Dynamics During the Differentiation of Embryonic Stem Cells in Living Subjects. Molecular Imaging and Biology, 2014, 16, 865-876.	2.6	12
124	Dual Reporter Gene Imaging for Tracking Macrophage Migration Using the Human Sodium Iodide Symporter and an Enhanced Firefly Luciferase in a Murine Inflammation Model. Molecular Imaging and Biology, 2013, 15, 703-712.	2.6	31
125	Combined RNA interference of adenine nucleotide translocase-2 and ganciclovir therapy in hepatocellular carcinoma. Nuclear Medicine and Biology, 2013, 40, 987-993.	0.6	3
126	Biliary Flow in Septate Gallbladder on Hepatobiliary Scintigraphy with SPECT/CT. Nuclear Medicine and Molecular Imaging, 2013, 47, 220-221.	1.0	0

#	Article	IF	CITATIONS
127	Salivary Gland Function 5 Years After Radioactive Iodine Ablation in Patients with Differentiated Thyroid Cancer: Direct Comparison of Pre- and Postablation Scintigraphies and Their Relation to Xerostomia Symptoms. Thyroid, 2013, 23, 609-616.	4.5	117
128	Estimation of True Serum Thyroglobulin Concentration Using Simultaneous Measurement of Serum Antithyroglobulin Antibody. International Journal of Endocrinology, 2013, 2013, 1-7.	1.5	12
129	In Vivo Monitoring of Survival and Proliferation of Hair Stem Cells in a Hair Follicle Generation Animal Model. Molecular Imaging, 2013, 12, 7290.2012.00046.	1.4	5
130	Effect of Parotid Gland Massage on Parotid Gland Tc-99m Pertechnetate Uptake. Thyroid, 2012, 22, 611-616.	4.5	15
131	Sodium Iodide Symporter for Nuclear Molecular Imaging and Gene Therapy: From Bedside to Bench and Back. Theranostics, 2012, 2, 392-402.	10.0	100
132	Implications of Three-Phase Bone Scintigraphy for the Diagnosis of Bisphosphonate-Related Osteonecrosis of the Jaw. Nuclear Medicine and Molecular Imaging, 2012, 46, 162-168.	1.0	20
133	A Case of Metastatic Endobronchial Melanoma from an Unknown Primary Site. Tuberculosis and Respiratory Diseases, 2012, 72, 169.	1.8	1
134	Prognostic implications of microscopic involvement of surgical resection margin in patients with differentiated papillary thyroid cancer after high-dose radioactive iodine ablation. Annals of Nuclear Medicine, 2012, 26, 311-318.	2.2	24
135	Multistage High-Dose I-131 Treatment for a Nonthyroidectomized Patient With Metastatic Differentiated Thyroid Cancer. Clinical Nuclear Medicine, 2011, 36, e224-e227.	1.3	3
136	Applications of Molecular Imaging in Drug Discovery and Development Process. Current Pharmaceutical Biotechnology, 2011, 12, 459-468.	1.6	30
137	Neurolymphomatosis on F-18 FDG PET/CT and MRI Findings: A Case Report. Nuclear Medicine and Molecular Imaging, 2011, 45, 76-78.	1.0	23
138	Prognostic Value of Primary Tumor Uptake on F-18 FDG PET/CT in Patients with Invasive Ductal Breast Cancer. Nuclear Medicine and Molecular Imaging, 2011, 45, 117-124.	1.0	44
139	Pulmonary Aspergilloma Mimicking Metastasis from Papillary Thyroid Cancer. Thyroid, 2011, 21, 555-558.	4.5	34
140	Combined <i>E7</i> -Dendritic Cell-Based Immunotherapy and Human Sodium/Iodide Symporter Radioiodine Gene Therapy with Monitoring of Antitumor Effects by Bioluminescent Imaging in a Mouse Model of Uterine Cervical Cancer. Cancer Biotherapy and Radiopharmaceuticals, 2011, 26, 671-679.	1.0	10
141	False-Positive Axillary Lymph Node on F-18 FDG PET/CT due to Moxibustion Therapy. Nuclear Medicine and Molecular Imaging, 2010, 44, 307-308.	1.0	0
142	Combined radionuclide–chemotherapy and in vivo imaging of hepatocellular carcinoma cells after transfection of a triple-gene construct, NIS, HSV1-sr39tk, and EGFP. Cancer Letters, 2010, 290, 129-138.	7.2	15
143	Enhanced anti-tumor effects of combined MDR1 RNA interference and human sodium/iodide symporter (NIS) radioiodine gene therapy using an adenoviral system in a colon cancer model. Nature Precedings, 2009, , .	0.1	0
144	New quantitative method for bone tracer uptake of temporomandibular joint using Tc-99m MDP skull SPECT. Annals of Nuclear Medicine, 2009, 23, 651-656.	2.2	21

#	Article	IF	CITATIONS
145	Intense Accumulation of F-18 FDG in Colonic Wall in Adult Onset Still Disease With Pseudomembranous Colitis. Clinical Nuclear Medicine, 2008, 33, 806-808.	1.3	13